

# Multiple measurements of quasars acting as standard probes: model independent calibration and exploring the Dark Energy Equation of States

Xiaogang Zheng<sup>1</sup>, Shuo Cao<sup>2\*</sup>, Marek Biesiada<sup>2,3</sup>, Xiaolei Li<sup>4</sup>, Tonghua Liu<sup>2</sup>, and Yuting Liu<sup>2</sup>

*1. School of Electrical and Electronic Engineering,  
Wuhan Polytechnic University, Wuhan 430023, China;*

*2. Department of Astronomy, Beijing Normal University, 100875, Beijing, China; caoshuo@bnu.edu.cn*

*3. National Centre for Nuclear Research, Pasteura 7, 02-093 Warsaw, Poland;*

*4. College of Physics, Hebei Normal University, Shijiazhuang 050024, China*

Recently, two classes of quasar samples were identified, which are promising as new cosmological probes extending to higher redshifts. The first sample uses the nonlinear relation between the ultraviolet and X-ray luminosities of quasars to derive luminosity distances, whereas the linear sizes of compact radio quasars in the second sample can serve as standardized rulers, providing angular-diameter distances. In this study, under the assumption of a flat universe, we refreshed the calibration of multiple measurements of high-redshift quasars (in the framework of a cosmological-model-independent method with the newest Hubble parameters data). Furthermore, we placed constraints on four models that characterize the cosmic equation of state ( $w$ ). The obtained results show that: 1) the two quasar samples could provide promising complementary probes at much higher redshifts, whereas compact radio quasars perform better than ultraviolet and X-ray quasars at the current observational level; 2) strong degeneracy between the cosmic equation of state ( $w$ ) and Hubble constant ( $H_0$ ) is revealed, which highlights the importance of independent determination of  $H_0$  from time-delay measurements of strongly lensed Quasars; 3) together with other standard ruler probes, such as baryon acoustic oscillation distance measurements, the combined QSO+BAO measurements are consistent with the standard  $\Lambda$ CDM model at a constant equation of state  $w = -1$ ; 4) ranking the cosmological models, the polynomial parametrization gives a rather good fit among the four cosmic-equation-of-state models, whereas the Jassal-Bagla-Padmanabhan (JBP) parametrization is substantially penalized by the Akaike Information Criterion and Bayesian Information Criterion criterion.

## I. INTRODUCTION

Observing the type-Ia Supernovae has revealed the accelerated expansion of the universe [1, 2], and the follow-up projects have further supported the idea [3–5]. This phenomenon is supported by the increase in observational evidence such as the cosmic microwave background (CMB) anisotropies [6–8], baryon acoustic oscillation (BAO) [9, 10], Hubble parameters derived from passively evolving galaxies [11, 12], and Einstein radius measurements of strong lensing systems [13, 14]. The simplest way to describe the cosmic acceleration phenomenon is to adopt the  $\Lambda$ CDM model, in which the cosmological constant  $\Lambda$  represents the negative-pressure dark energy (DE). However, there are still the same problems under the assumption of this simple model, including the well-known theoretical difficulties of coincidence and the fine-tuning problems. From the observational perspective, the values of the Hubble constant obtained from the measurements of local supernova through the SH0ES collaboration [15, 16] are in tension with the *Planck* CMB data analyzed under the assumption of a flat  $\Lambda$ CDM model [7, 8]. The  $H_0$  value derived from gravitational lensing time-delay distances [17] under the assumption of a flat  $\Lambda$ CDM model is also in tension with the estimates of the early universe [7]. Recently, some other observational data, including the Hubble parameter measurements [18] and quasars calibrated as standard candles [19], were observed to be in tension with the  $\Lambda$ CDM model, especially in the so-called “redshift desert” region. Moreover, another important issue is whether the DE equation-of-state (EoS) parameter evolves with redshifts [20].

Currently, most of the cosmological observations refer to either low [3–5] or high redshift [6–8] regions. The so-called “redshift desert” makes it difficult to study the dynamical evolution of DE. Consequently, a promising probe could be quasars, which are the brightest objects in the universe seen at very high redshifts. Although using quasars as standard cosmological probes is ambiguous, it was proposed that luminosity distances can be assessed from the radius of the broad-line region (BLR)-the monochromatic luminosity relation [21, 22], the properties of the super-Eddington accreting massive black holes [23], the correlation between the X-ray variability amplitude and the mass of the black hole [24], or the nonlinear relation between the ultraviolet (UV) and X-ray luminosities [19, 25]. Meanwhile, the angular-diameter distances can be derived from the classical geometrical size of the BLR [26], the angular size-redshift relation of compact structures in intermediate-luminosity radio quasars [27–29], etc. Taking advantage of the available rich samples, we employed the nonlinear relation between the UV and X-ray flux measurements of quasars [19], and the angular size-redshift relation from compact radio quasars [27]. Besides the large dispersion of the data points, these two compilations of quasar suffer from the ambiguity in the meaning of nuisance parameters, which

should be calibrated with external probes. However, benefiting from their broad redshift coverage, they have the potential to address the issues of the dynamical evolution of DE, the measurements of the speed of light [30], and cosmic curvature at higher redshifts [31], and the testing of the cosmic-distance-duality relation in the early universe [32].

In this study, we take advantage of the high redshift coverage for both the Hubble parameters derived from differential ages of passively evolving galaxies (so-called cosmic chronometers) [11, 12] and the two different kinds of quasar samples [19, 27]. First, we refreshed the calibration of the nuisance parameters in the nonlinear relation between the UV and X-ray luminosity of quasars (QSO[XUV] hereafter) and that in the angular size-redshift relation of the compact structure sizes in radio quasars (QSO[CRS]). This was performed in a nonparametric, model-independent technique developed by ref.[33]. Because the redshift coverage of the Hubble parameters ( $0.07 < z < 1.965$ ) is smaller in both quasar samples,  $0.462 < z < 2.73$  for QSO[CRS] [27] and  $0.036 < z < 5.1003$  for QSO[XUV] [19], we extended the calibrated nuisance parameters and applied them to the redshift range larger than the  $H(z)$  sample. We compared two quasar samples with regard to their ability to constrain cosmological model parameters. In particular, we studied different parametrizations of the cosmic equation of state (EoS), combined with the current BAO data and Hubble constant priors.

In Section II, we introduce two kinds of quasar samples and calibrate their nuisance parameters. Then, in Section III, we introduce four parametrizations of DE EoS allowed to evolve in redshifts and test them with the calibrated quasar samples combined with the BAO data. The results are discussed in Section IV and the conclusions are presented in Section V.

## II. MODEL INDEPENDENT CALIBRATION OF QUASAR SAMPLES

The redshift range probed by quasar measurements has a wide coverage, but such data can hardly be used directly as a standard cosmological probe because quasars have neither standard luminosity nor a clearly defined size scale. Recently, interesting methods that provide the luminosity distance and angular-diameter distance by quasars through multiband observations have been proposed, including the nonlinear relation between the UV and X-ray luminosities of quasars [19, 25] and the angular size-redshift relation of the compact radio structure [27, 28], respectively.

According to the empirical relation between the UV and X-ray luminosities of quasars,  $\log(L_X) = \gamma \log(L_{UV}) + \beta$  (for details, see ref.[19, 25]), and the flux-luminosity relation of  $F_\nu = L_\nu/4\pi D_L^2$ , one can relate the respective fluxes (observable quantities) with the luminosity distance thus:

$$\begin{aligned} \log(F_X) &\equiv \Phi(\log F_{UV}, D_L) \\ &= \beta' + \gamma \log(F_{UV}) + 2(\gamma - 1) \log(D_L(z; \mathbf{p})) \end{aligned} \quad (1)$$

where  $\beta' = \beta + (\gamma - 1)\log(4\pi)$  is the effective intercept, which is defined as the combination of the intercept  $\beta$  and the slope  $\gamma$ . In this formula, the unit of flux densities  $F_X$  and  $F_{UV}$  is  $\text{erg s}^{-1} \text{cm}^{-2} \text{Hz}^{-1}$ , and that luminosity distances is Mpc. In principle, the luminosity distance in Eq.(1) is the true one and can be confronted with the theoretically predicted one  $D_L(z; \mathbf{p})$ , where  $\mathbf{p}$  denotes all cosmological model parameters. To test cosmological models, one needs the prior knowledge of the  $\beta$  and  $\gamma$  coefficients. In other words, one needs to calibrate this relation in a cosmological model independent way. As discussed in a later section, we employed  $D_L(z)$  obtained from  $H(z)$  measurements provided by cosmic chronometers. Another option could be a joined assessment of the nuisance parameters with the cosmological parameters during the investigation [32, 34–38]. As discussed in [25], a slope parameter  $\gamma$  can be fitted on the subsamples covering different redshift bins across the full redshift range of the data. It has the advantage of being able to test whether the  $\gamma$  parameter evolves with redshifts, and if it does not, one can estimate the effective slope as an average over the bins. It is different in the case of the intercept parameter  $\beta$ , which is hard to check without having a deep physical understanding of the nonlinear luminosity relation. Moreover, the data points are still largely scattered despite the that, in the compiled sample used herein, the scatter has already been significantly reduced. Therefore, in the statistical analysis, we also included another nuisance parameter  $\delta$ , which describes this scatter.

To obtain reliable information on the cosmological model, a reasonable prior of nuisance parameters calibrated from more precise external probes is necessary. We optimized the nuisance parameters using the luminosity distances from the model independent of the Gaussian Process by minimizing the likelihood the function

$$\begin{aligned} \ln \mathcal{L}_{QSO[XUV]} &= -\frac{1}{2} \sum_i^N \\ &\quad \left\{ \frac{[\log(F_X)_i - \Phi(\log F_{UV}, D_L)]^2}{s_i^2} + \ln(2\pi s_i^2) \right\} \end{aligned} \quad (2)$$

where the expression  $\Phi(F_{UV}, D_L)$  is given in Eq.(1) and the variance,  $s_i^2 = \sigma_i^2 + \delta_i^2$ , is the combination of  $\sigma_i$  and  $\delta_i$ , which denote the statistical uncertainties and the intrinsic scatter, respectively. To calibrate the nuisance parameters, ( $\gamma$  and  $\beta$ ), the statistical uncertainties include  $\sigma(\log F_X)$  and  $\sigma(D_L)$ , which denote the uncertainties of the observed  $\log F_X$  and reconstructed  $D_L$ , respectively. Namely,  $\sigma_i^2 = \sigma(\log F_X)_i^2 + (\frac{2(\gamma-1)}{D_L \ln 10} \sigma(D_L))_i^2$ . For the investigation of the DE EoS, the statistical uncertainty include  $\sigma(\log F_X)$  and the gaussian priors are assumed for the nuisance parameters. As discussed in ref.[19], the uncertainty of  $F_{UV}$  is negligible compared to that of  $F_X$ , and consequently, it is ignored herein. In ref.[25], the "best sample" of 808 quasars was extracted for cosmology inference, and the sample was enlarged to 1598 in ref.[19], and that was employed in this study.

On the other hand, another quasar sample obtained through radio observations was proposed to provide angular-diameter distances using the simple angular size ( $\theta$ )-redshift ( $z$ ) relation [39–41]. The angular size at different redshifts  $\theta(z)$  can be expressed in terms of the intrinsic metric size  $l_m$  of the compact radio structure of quasars and the angular-diameter distances  $D_A(z)$  as follows:

$$\theta(z) = \frac{l_m}{D_A(z)} \quad (3)$$

where  $l_m$  may depend on the luminosity of the source or evolve with redshifts. In ref.[27, 28], a sample of 120 intermediate-luminosity radio quasars with negligible dependence on both luminosity and redshift was identified. Thus, the intrinsic metric length  $l_m$  can be taken simply as the linear size parameter  $l$ . To calibrate the linear size using the cosmological model independent  $H(z)$  data, we maximized the likelihood function defined as:

$$\ln \mathcal{L}_{QSO[CRS]} = -\frac{1}{2} \sum_{i=1}^{120} \frac{[\theta_{obs}(z_i) - \theta_{th}(z_i)]^2}{\sigma_{\theta(z_i)}^2} \quad (4)$$

where the variance,  $\sigma_{\theta(z_i)}^2 = [\sigma_{\theta(z_i)}^{sta}]^2 + [\sigma_{\theta(z_i)}^{sys}]^2$ , includes the statistical and 10% systematic uncertainties. This method is abbreviated as the subscript, QSO[CRS]. To calibrate the linear-size parameter, the statistical uncertainties include two terms: one from the observed angular size and the other propagated from the reconstructed angular-diameter distance, i.e.,  $[\sigma_{\theta(z_i)}]^2 = [\sigma(\theta_{obs}(z_i))]^2 + [\frac{l}{D_A(z_i)} \sigma(D_A(z_i))]^2$ . To investigate DE EoS, rather than the uncertainty of the reconstructed angular-diameter distance  $\sigma(D_A)$ , that of the calibrated linear size  $\sigma(l)$  was considered. Such methodology has been extensively employed in subsequent cosmological studies of intermediate-luminosity radio quasars [42–44]

Lastly, as already mentioned above, the cosmic expansion rates  $H(z)$  were used to calibrate the nuisance parameters. The sample used was obtained through the cosmological-model-independent method using the so-called cosmic chronometers [11, 12]. The idea is that  $H(z) = \frac{\dot{a}}{a} = -\frac{1}{1+z} \frac{dz}{dt}$ , which is expressed in terms of observable quantities (i.e., redshifts and their change over time), could be obtained without assuming any particular cosmological model. The point here is to measure  $dz/dt$  directly, which could be achieved using massive, early-type galaxies that evolve passively on a timescale longer than their age difference. Certain features of their spectra, such as D4000 that breaks at 4000Å, which indicates the evolution of their stellar populations, enable us to measure the age difference of such galaxies. As discussed in ref.[27], the choice of a stellar-population-synthesis model may strongly affect the estimates of the age difference at higher redshifts  $z > 1.2$ . Hence, only 24 data points, up to  $z < 1.2$ , were considered in ref.[27]. The redshift coverage of both the above-mentioned quasar samples is much broader than  $H(z)$  measurements. Moreover, such a restriction would exclude a considerable fraction of angular size  $\theta(z)$  data and could affect the results of the calibrations. Therefore, we exploited a wider redshift range and used a total of 31  $H(z)$  measurements with redshifts of  $0.07 < z < 1.965$ .

From the observed data, we reconstructed the  $H(z)$  function in the redshift range  $0 < z < 2$  using a model-independent method of Gaussian Processes (GP). The Python package, GaPP, developed in ref.[33] and used in ref.[32, 45], was employed in the reconstruction, assuming zero-mean and squared exponential-covariance functions. The effects of the mean function and covariance selection were discussed in our previous study [32], where it was shown that the choice of the covariance function does not have a significant influence on the results, and the impact of the mean-function choice was even smaller. The results are shown in Fig.(1), where the red points with the error bars, the green dashed line, and the green regions with different transparency indicates the 31  $H(z)$  measurements, GP reconstructed  $H(z)$ , and corresponding confidence regions, respectively. Moreover, different reconstruction methods may also affect the results and subsequent calibration. To show the impact of such methods, we performed reconstruction separately using the Bézier parametric curve of degree  $n = 2$ , which was used to investigate the Amati relation [46], and the log-polynomial form employed in QSO[XUV] studies [19]. More specifically,  $H^{Bez}(z) = \beta_0(1 - \frac{z}{z_m})^2 + 2\beta_1 \frac{z}{z_m}(1 - \frac{z}{z_m}) + \beta_2(\frac{z}{z_m})^2$  and  $H^{Pol}(z) = H_0[\log(1+z) + a_2 \log^2(1+z) + a_3 \log^3(1+z)]$ . The reconstruction results are shown in Fig.(1), where the cyan dash-dot line indicates the  $H(z)$  reconstructed from the Bézier parametric curve and the

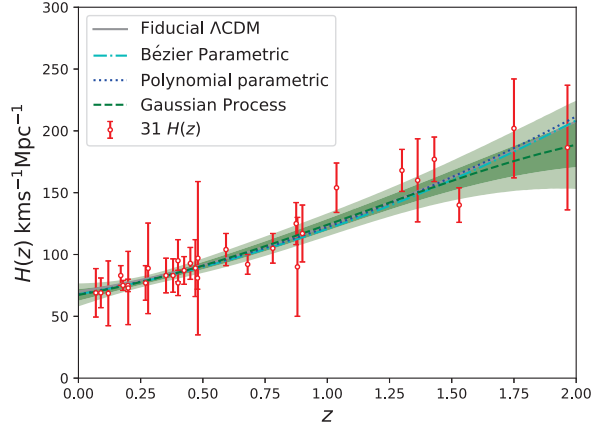


FIG. 1: The observed Hubble parameters and reconstructed expansion rate up to the redshift  $z = 2$ . The red points with error bars represent the  $H(z)$  measurements obtained using cosmic chronometers and the green dashed line indicates the  $H(z)$  function reconstructed with Gaussian Processes, and it is surrounded by the green region of various transparencies corresponding to the  $1\sigma$  and  $2\sigma$  confidence region. For comparison, we added the theoretical prediction from a fiducial flat  $\Lambda$ CDM model with the Hubble constant  $H_0 = 70 \text{ km s}^{-1} \text{ Mpc}^{-1}$  and matter-density parameter  $\Omega_m = 0.3$  (gray line), the reconstructed  $H(z)$  from the Bézier parametric curve (cyan dash-dot line), and that from log-polynomial parameterization (blue dotted line).

blue dotted line indicates that from the log-polynomial parametrization. Their confidence regions are not shown so as not to blur the picture since they are similar to that from the Gaussian process. The theoretical prediction from a fiducial flat  $\Lambda$ CDM model with the Hubble constant  $H_0 = 70 \text{ km s}^{-1} \text{ Mpc}^{-1}$  and matter-density parameter  $\Omega_m = 0.3$  was also performed for comparison. Despite that the reconstructed  $H(z)$  was more consistent with the theoretical prediction from the fiducial model, both of them encountered the problem of order truncation, which may affect the results, especially at high redshifts [47, 48], and we preferred to use the GP method in this study. Through GP, we also obtained the Hubble constant  $H(z = 0) = 67.32 \pm 4.7 \text{ km s}^{-1} \text{ Mpc}^{-1}$ , which will be used later. The result of the reconstruction is consistent with that using only the 31 cosmic chronometric measurements reported in [37, 49]. Furthermore, combining these 31  $H(z)$  measurements with the latest SN Ia compilations (Pantheon and MCT), ref.[50] obtained a more accurate value for the Hubble constant with the best value consistent with that of ref.[37, 49], whereas we only considered the application of 31  $H(z)$  measurements herein.

Once we obtain the reconstructed  $H(z)$ , we can derive the cosmological distances. As reported in ref.[51], under the assumption of flat universe, the comoving distance can be calculated from the reconstructed  $H(z)$  using the usual simple trapezoidal rule:

$$D(z) = c \int_0^z \frac{dz'}{H(z')} \approx \frac{c}{2} \sum_{i=1}^n (z_{i+1} - z_i) \left[ \frac{1}{H(z_{i+1})} + \frac{1}{H(z_i)} \right] \quad (5)$$

and the corresponding uncertainty is given by

$$\delta D(z) = \frac{c}{2} \sum_{i=1}^n (z_{i+1} - z_i) \left( \frac{\sigma_{H_{i+1}}^2}{H_{i+1}^4} + \frac{\sigma_{H_i}^2}{H_i^4} \right)^{1/2} \quad (6)$$

Then, the angular-diameter and luminosity distances can be calculated as  $D_A(z) = D(z)/(1+z)$  and  $D_L(z) = D(z)(1+z)$ , respectively.

Matching the distances reconstructed from  $H(z)$  with the data from both QSO samples, the totals of 1330 and 106 data pairs were selected for QSO[XUV] and QSO[CRS], respectively. The samples were calibrated with a maximum likelihood approach based on Eq.(2) and Eq.(4), as illustrated in Fig.(2) and Fig.(3). The best-fitted values of the slope parameter  $\gamma = 0.634 \pm 0.011$ , intercept parameter  $\beta = 7.75 \pm 0.34$ , and dispersion  $\delta = 0.232 \pm 0.005$  for the QSO[XUV] sample were considered as the calibrated results and employed in the investigation of DE EoS as the Gaussian priors. Comparing with some previous works, the results obtained in study are consistent with the  $\gamma = 0.633 \pm 0.002$  and  $\delta = 0.24$  from a best-fit log-linear model in ref.[19] and the  $\gamma = 0.62 \pm 0.01$  and  $\delta = 0.23 \pm 0.004$  obtained under the assumption of a flat  $\Lambda$ CDM model by ref.[36]. The intercept parameter  $\beta$  is fully dependent on external calibrators;

hence, it is harder to compare. However, the obtained value is consistent with that of the fits reported in ref.[36]. For direct cosmological investigations, one needs to determine the cosmological distances at the corresponding redshifts. For the 1598 QSO[XUV] sample [19] used in this study, the luminosity distance can be computed using Eq.(1) as

$$\log D_L = \frac{[\log F_X - \gamma \log F_{UV} - \beta - (\gamma - 1) \log(4\pi)]}{2(\gamma - 1)} \quad (7)$$

The distance modulus is given by

$$\begin{aligned} \mu &= 5 \log D_L + 25 \\ &= \frac{5}{2(\gamma - 1)} [\log F_X - \gamma \log F_{UV} - \beta - (\gamma - 1) \log(4\pi)] + 25 \end{aligned} \quad (8)$$

and the corresponding uncertainty is given by

$$\begin{aligned} \sigma(\mu) &= \frac{5}{2(\gamma-1)} \left[ \sigma(\log F_X)^2 + \sigma(\beta)^2 \right. \\ &\quad \left. + \left( \frac{\log F_{UV} - \log F_X + \beta}{\gamma-1} \sigma(\gamma) \right)^2 \right]^{1/2} \end{aligned} \quad (9)$$

The derived distance modulus and the corresponding uncertainties are shown in the left panel of Fig.(4), where  $\sigma(\gamma)$  and  $\sigma(\beta)$  are taken as  $1\sigma$  uncertainties from the aforementioned calibration results, as shown in the right panel of Fig.(2). Owing to the large dispersion of distance modulus, another scatter parameter could be introduced for the likelihood calculation of  $\mu$ . In this study, we preferred to use the likelihood Eq.(2) directly with the Gaussian priors on the nuisance parameters ( $\gamma$  and  $\beta$ ) and intrinsic scatter ( $\delta$ ).

For the linear size, the best-fitted value was  $l = 10.89 \pm 0.19 pc$ . It is somewhat smaller than but marginally consistent with that calibrated with the Union2.1 SN Ia compilation,  $l = 11.42 \pm 0.28 pc$ , in ref.[27] and that calibrated on a subsample of  $H(z)$  measurements covering redshifts  $z < 1.2$  in ref.[28] ( $l = 11.03 \pm 0.25$ ). With the measurements of the angular size and the calibrated linear size, the angular-diameter distance and the corresponding uncertainties can be calculated as  $D_A(z) = l/\theta(z)$  and  $\sigma(D_A) = [(\sigma(l)/\theta)^2 + (l\sigma(\theta)/\theta^2)^2]^{1/2}$ . The calculated results are shown in the right panel of Fig.(4).

Comparing the measurements of the lower ( $0 < z < 2$ ) and the higher redshifts ( $z > 2$ ), the  $\log F_X - \log F_{UV}$  correlation of QSO[XUV] appears redshift dependent (the left panel of Fig.(2)) and the angular size  $\theta(z)$  seems larger and the angular-diameter distance  $D_A(z)$  smaller than the average value (the left panel of Fig.(3) and the right panel of Fig. (4), respectively). Considering the uncertainties of  $\log F_X$ , the slopes are similar, and the intercepts are different. This is consistent with the evolution discussion of the nuisance parameters in ref.[19] (their supplementary Fig. 8). The lack of  $\theta(z)$  measurements at higher redshifts may affect the QSO[CRS] approach. It should be noted that the sparsity of the current  $H(z)$  data at higher redshifts may affect the reliability of calibration, particularly in light of using them outside the redshift range of the actual calibration. Hence, there is hope that the data on Hubble parameters would be extended in the future to higher redshift ranges.

### III. INVESTIGATION OF THE DARK ENERGY EQUATION OF STATE

DE is synonymous with the unknown cause of the accelerated expansion of the universe. Since it is still unknown and we strive toward resolving the enigma, a useful approach is to model it as a fluid with some EoS:  $p = w\rho$ , where  $p$  is the pressure and  $\rho$  the energy density. The simplest model used in this context is the  $\Lambda$ CDM model, where the cosmological constant  $\Lambda$  – an entity having a long history in cosmology – represents DE. Formally, this was equivalent to  $w = -1$ . A somewhat more complicated model of DE is the so-called  $w$ CDM model, where the  $w$  coefficient is also a constant but different from  $\Lambda$ . These models can be classified into quintessence models ( $-1 < w < -1/3$ ), including phantom models ( $w < -1$ ) and quintom model, with  $w$  crossing the  $-1$  value. Most of the observations are very well consistent with the  $\Lambda$ CDM model, but significant deviation from it is still allowed according to their accuracy and precision. The crucial issue here is whether the cosmic EoS evolves in time (i.e., in redshift). Such unambiguous finding would be of utmost importance for theoretical studies, where a more fundamental explanation of DE is sought for, and the only (or one of the very few) common points with the real observational data could be the effective  $w$  parameter, not necessarily a constant. Below, we present four particular parametrizations of evolving EoS in flat universe to be studied in order to find out if and to what extent they are supported by QSO data combined with BAO measurements.

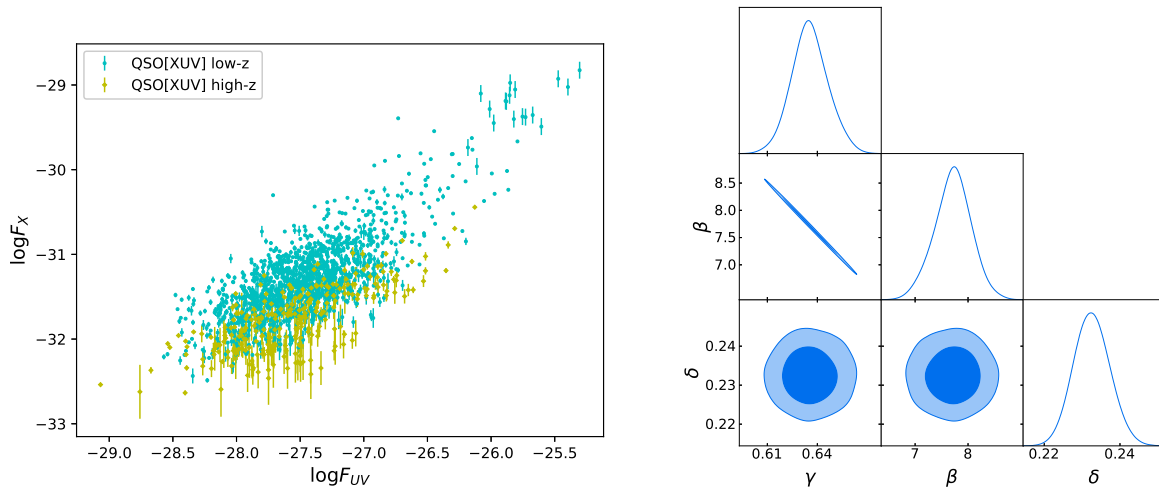


FIG. 2: Calibration of QSO[XUV] nuisance parameters with external  $H(z)$  measurements. Left: The flux relation between  $\log F_X$  and  $\log F_{UV}$ , where the cyan circle points correspond to the data matched with the reconstructed  $H(z < 2.0)$  used during the calibration. Yellow diamond points represent the rest of the sample. Right: Two-dimensional confidence regions and marginal distributions for the calibrated parameters: the slope parameter  $\gamma = 0.634 \pm 0.011$ , the intercept  $\beta = 7.75 \pm 0.34$  and dispersion  $\delta = 0.232 \pm 0.005$  for QSO[XUV] sample.

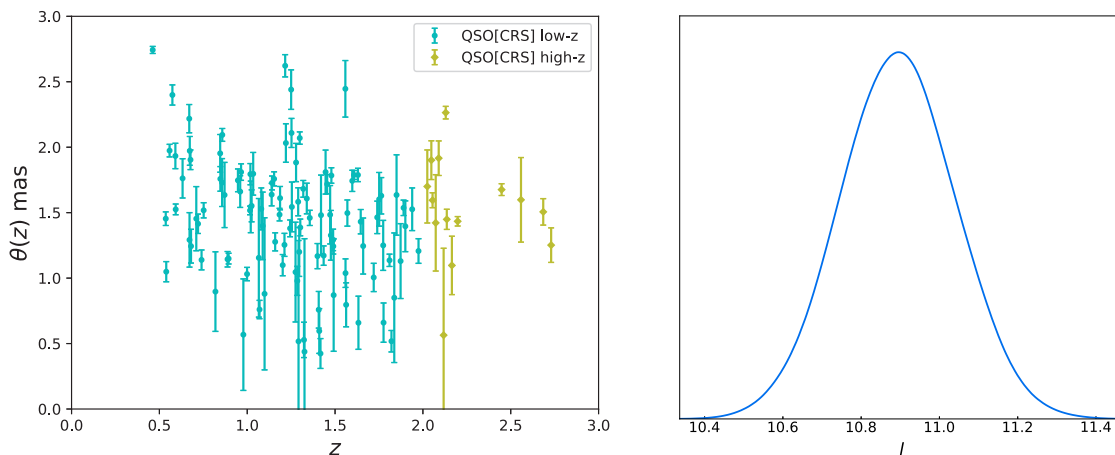


FIG. 3: Calibration of QSO[CRS] linear size parameter with external  $H(z)$  measurements. Left: Observed angular size-redshift relation of intermediate-luminosity quasars, where the points matched with the reconstructed  $H(z < 2.0)$  are displayed in cyan circle. Yellow diamond points represent the rest of the sample. Right: Probability distribution of the best-fitted linear size parameter  $l = 10.89 \pm 0.19$  pc.

### A. DE EoS parametrizations

To investigate the dynamical evolution of DE, which could be manifested as an EoS coefficient dependent on redshift  $w(z)$ , several phenomenological parameterizations have been proposed. Since none of them is clearly supported by a theoretical model, we chose just four of them. The simplest phenomenology could be just a first-order Taylor expansion:  $w(z) = w_0 + w_a z$ . It is divergent at redshifts  $z > 1$  and refers to the observable quantity  $z$ , which is not a physical degree of freedom like the scale factor  $a(t)$ . The same idea of Taylor expansion, but in  $a(t)$  rephrased in terms of  $z$ , led to the most widely used form of DE EoS, i.e., the Chevallier-Polarski-Linder (CPL) parametrization

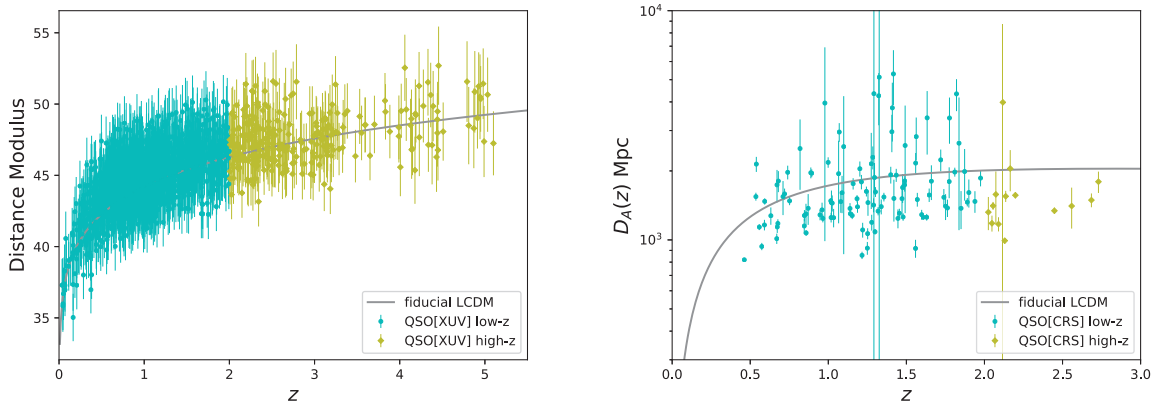


FIG. 4: Distance modulus of QSO[XUV] (left) and angular-diameter distances of QSO[CRS] (right) calculated using the prior values of the calibrated nuisance parameters. The cyan circle points correspond to the data used for the calibration of the nuisance parameter and the yellow diamond points represent the higher-redshift sample. The theoretical prediction from the fiducial flat  $\Lambda$ CDM model with the Hubble constant  $H_0 = 70 \text{ km s}^{-1} \text{ Mpc}^{-1}$  and density parameter  $\Omega_m = 0.3$  is indicated by the gray line for comparison.

[52, 53]

$$w(z) = w_0 + w_a \frac{z}{1+z}. \quad (10)$$

This parametrization has several advantages [53] such as well-bounded behavior at high redshifts, simple physical interpretations, and manageable two-dimensional phase space. However, it is also associated with some problems: it will encounter divergency in the future as  $z \sim -1$ ; the various limit values at low- $z$  ( $w(z \rightarrow 0) \sim w_0$ ) and high- $z$  ( $w(z \rightarrow \infty) \sim w_0 + w_a$ ), etc. Similar to the CPL parametrization, the JBP parametrization [54] was proposed as

$$w(z) = w_0 + w_a \frac{z}{(1+z)^2} \quad (11)$$

and it has the same DE EoS at present ( $z \rightarrow 0$ ) or remote past ( $z \rightarrow \infty$ ), with rapid variation at low- $z$ . For comparison, we also discuss the logarithmic parametrization [55]

$$w(z) = w_0 + w_a \ln(1+z) \quad (12)$$

This becomes infinite when  $z \rightarrow \infty$  under the assumption of the DE EoS. So, it can describe the behavior of DE when the redshift is not so high. Similarly to the method of fitting the Hubble diagram with a polynomial function applied in ref.[19], we investigated the polynomial parametrization [56]:

$$w(z) = -1 + w_0(1+z) + w_a(1+z)^2 \quad (13)$$

The dimensionless expansion rate  $E(z)$  can be calculated from the Friedman equation. A combined expression for

this (squared) in the above described EoS parametrizations is as follows:

$$\begin{aligned}
\text{CPL : } E^2(z) &= \Omega_m(1+z)^3 + (1-\Omega_m) \\
&\quad (1+z)^{3(1+w_0+w_a)} \exp\left[-\frac{3w_a z}{1+z}\right]; \\
\text{JBP : } E^2(z) &= \Omega_m(1+z)^3 + (1-\Omega_m) \\
&\quad (1+z)^{3(1+w_0)} \exp\left[\frac{3w_a z^2}{2(1+z)^2}\right]; \\
\text{Logarithmic : } E^2(z) &= \Omega_m(1+z)^3 + (1-\Omega_m) \\
&\quad (1+z)^{3(1+w_0)} \exp\left[\frac{3w_a}{2}(\ln(1+z))^2\right]; \\
\text{Polynomial : } E^2(z) &= \Omega_m(1+z)^3 + (1-\Omega_m) \\
&\quad \exp\left[3(w_0+w_a)z + 1.5w_a z^2\right].
\end{aligned} \tag{14}$$

The confrontation of the above listed expansion rate  $E(z)$  with QSO data would involve distances  $D_A(z) = D(z)/(1+z)$  and  $D_L(z) = D(z)(1+z)$ , where the comoving distance reads

$$D(z) = \begin{cases} \frac{c}{H_0 \sqrt{|\Omega_k|}} \sinh\left[\sqrt{|\Omega_k|} \int_0^z \frac{dz'}{E(z')}\right] & \text{for } \Omega_K > 0, \\ \frac{c}{H_0} \int_0^z \frac{dz'}{E(z')} & \text{for } \Omega_K = 0, \\ \frac{c}{H_0 \sqrt{|\Omega_k|}} \sin\left[\sqrt{|\Omega_k|} \int_0^z \frac{dz'}{E(z')}\right] & \text{for } \Omega_K < 0. \end{cases} \tag{15}$$

The curvature parameter  $\Omega_k$  is expressed in terms of  $K$  as  $\Omega_k = -c^2 K / (a_0 H_0)^2$ , where  $c$  is the speed of light. Current cosmological observations favor the flat universe ( $\Omega_k = 0.001 \pm 0.002$ )[7]; thus, we assumed the flat universe in this study. Moreover, ref.[38] used time-delay lenses and 1598 QSO[XUV] to estimate the curvature and found  $\Omega_k = -0.01_{-0.17}^{+0.18}$ , which supports the validity of our assumption.

## B. Model Constraint and Selection

As mentioned in Section II, the strategy employed herein is to fit the free parameters of the four models introduced above to the QSO[XUV] and QSO[CRS] data. Therefore, we employed the likelihoods Eq.(2) and Eq.(4). However, we fixed the nuisance parameters at the calibrated values and let the distances depend on cosmic EoS parameters.

To show the constraint ability of quasar samples in comparison and combination with other standard cosmological probes, we included the most recent BAO measurements and assume a Gaussian prior for the Hubble constant of  $H_0 = 67.32 \pm 4.7 \text{ km s}^{-1} \text{ Mpc}^{-1}$  from the GP  $H(z)$  reconstruction. The likelihood function for the uncorrelated BAO measurements can be expressed as

$$\ln \mathcal{L}_{\text{BAO}}(\mathbf{p}) = -\frac{1}{2} \sum_i^5 \frac{[A_{th}(\mathbf{p}; z_i) - A_{obs}(z_i)]^2}{\sigma_{A_i}^2} \tag{16}$$

and for the correlated measurements

$$\ln \mathcal{L}_{\text{BAO}}(\mathbf{p}) = -\frac{1}{2} [\vec{A}_{th}(\mathbf{p}; z_i) - \vec{A}_{obs}(z_i)]^T C^{-1} [\vec{A}_{th}(\mathbf{p}; z_i) - \vec{A}_{obs}(z_i)] \tag{17}$$

where  $C^{-1}$  is the inverse of the covariance matrix

$$C = \begin{bmatrix} 624.707 & 23.729 & 325.332 & 8.34963 & 157.386 & 3.57778 \\ 23.729 & 5.60873 & 11.6429 & 2.33996 & 6.39263 & 0.968056 \\ 325.332 & 11.6429 & 905.777 & 29.3392 & 515.271 & 14.1013 \\ 8.34963 & 2.33996 & 29.3392 & 5.42327 & 16.1422 & 2.85334 \\ 157.386 & 6.39263 & 515.271 & 16.1422 & 1375.12 & 40.4327 \\ 3.57778 & 0.968056 & 14.1013 & 2.85334 & 40.4327 & 6.25936 \end{bmatrix} \tag{18}$$



For both uncorrelated and correlated BAO data, the quantities  $A_{obs}(z_i)$ ,  $\sigma_{A_i}$ , and  $A_{th}(z_i)$  denote the measurements, observational uncertainties, and theoretical expressions, respectively. Correlated quantities include the scaled transverse comoving distance,  $D_M(z)(r_{s, fid}/r_s)$ , and the scaled Hubble parameters,  $H(z)(r_s/r_{s, fid})$ , from the final galaxy-clustering data of the Baryon Oscillation Spectroscopic Survey (BOSS). Uncorrelated quantities include the distance ratio,  $r_s/D_V(z)$ ,  $D_V(z)(r_{s, fid}/r_s)$ , the Hubble distance,  $(D_H(z))^{0.7}(D_M(z))^{0.3}/r_s$ , and the BAO scale along the line of sight  $c/(r_s H(z))$  measurements from the 6dF Galaxy Survey, the Sloan Digital Sky Survey (SDSS) Data Release 7, the SDSS-IV extended Baryon Oscillation Spectroscopic Survey (eBOSS) Data Release 14, the SDSS Data Release 12, and the SDSS-III BOSS Data Release 11, respectively.  $D_V(z)$ ,  $D_H(z)$ ,  $D_M(z)$ , and  $H(z)$  denote the spherically averaged angular-diameter distance, Hubble distance, transverse comoving distance, and Hubble parameters, respectively. The quantity  $r_s$  denotes the size of the sound horizon at the drag epoch, and  $r_{s, fid}$  is the corresponding quantity from the original measurement. The detailed expressions and quantities can be found in the text and Table 1 of ref.[57], respectively.

The best-fitted values of cosmological EoS parameters  $\mathbf{p}$  can be determined by minimizing the chi-square objective function,  $\chi^2(\mathbf{p}) = -2 \ln \mathcal{L}(\mathbf{p})$ ; i.e., by maximizing the likelihood function. In the case of joint analysis, log-likelihoods (or equivalently chi-square functions) should be included (QSO and BAO data are independent).

As already stressed, the log-likelihoods depend on both the EoS parameters and the calibrated-nuisance parameters  $\nu$ . Since they have been fitted by an independent method with some accuracy, they should be rather marginalized over. Assuming that the prior distribution of  $\nu$ , i.e.,  $P(\nu)$ , is Gaussian with the mean  $\bar{\nu}$  and standard deviation  $\sigma_\nu$ :

$$P(\nu) = \frac{1}{\sqrt{2\pi\sigma_\nu^2}} e^{-(\nu-\bar{\nu})^2/(2\sigma_\nu^2)} \quad (19)$$

The posterior likelihood function can be obtained by integrating  $\mathcal{L}(\mathbf{p}, \nu)$  over  $P(\nu)$  as follows:

$$\mathcal{L}(\mathbf{p}) = \int_0^\infty \mathcal{L}(\mathbf{p}, \nu) P(\nu) d\nu \quad (20)$$

This is how we treated the calibrated nuisance parameters. More specifically, we assumed the following Gaussian (prior) distributions for the nuisance parameters:  $H_0 = \mathcal{N}(67.32, 4.7)$ ,  $\gamma = \mathcal{N}(0.634, 0.011)$ ,  $\beta = \mathcal{N}(7.75, 0.34)$  and  $\delta = \mathcal{N}(0.232, 0.005)$ . Next, we minimized the chi-square posterior (marginalized over the nuisance parameters)  $\chi_{min}^2(\mathbf{p}) = -2 \ln \mathcal{L}_{max}(\mathbf{p})$ , which is equivalent to maximizing the likelihood. One of our goals is to quantify the degree of support given to competing models (EoS parametrizations) by the data. While the standard metric, like the chi-square per degree of freedom ( $\chi^2/d.o.f.$ ), describes the goodness of fit, it is insufficient to compare the models. Therefore, we employed also two specific model selection techniques [58]: the Akaike Information Criterion (AIC)

$$AIC = \chi_{min}^2 + 2k \quad (21)$$

and the Bayesian Information Criterion (BIC)

$$BIC = \chi_{min}^2 + k \ln N \quad (22)$$

The AIC value for a single model is useless; what is useful instead are the differences,  $\Delta_i(AIC) = AIC_i - AIC_{min}$ , calculated over the whole set of alternative candidate models ( $\mathcal{M}_i$ ;  $i = 1, \dots, M$ ) where by  $AIC_{min}$  we denote as  $\min\{AIC_i; i = 1, \dots, M\}$ . The relative strength of the evidence for each model can be calculated as the likelihood of the model given the data  $\mathcal{L}(\mathcal{M}_i|data) \sim \exp(-\frac{1}{2}\Delta_i)$ . The relative likelihoods of the models,  $\mathcal{L}(\mathcal{M}_i|data)$ , normalized to unity are termed Akaike weights  $w_i$ , i.e.,  $w_i = \exp\{-\frac{1}{2}\Delta_i\} / \sum_{i=1}^M \exp\{-\frac{1}{2}\Delta_i\}$ . In Bayesian language, an Akaike weight corresponds to the posterior probability of a model (under the assumption of equal prior probabilities). The (relative) evidence for the models can also be determined by the evidence ratios of model pairs as  $\frac{w_i}{w_j} = \frac{\mathcal{L}(\mathcal{M}_i|data)}{\mathcal{L}(\mathcal{M}_j|data)}$ . The evidence ratios is substantiated as odds against the given model with respect to the best one.

#### IV. RESULTS AND DISCUSSION

The constraints for the  $w$ CDM model obtained through distance measurements of two subsamples of QSO[XUV], independent quasar samples (XUV or CRS) and both QSO samples combined with BAO are shown in Fig.(5). The 2D marginalized contours with  $1\sigma$  and  $2\sigma$  uncertainties from different samples are shown, both to compare the lower and higher redshift subsamples of QSO[XUV] and the constraints from different observations. In the left panel of Fig.(5), the filled cyan and the yellow contours indicate the constraints from the 1330 lower redshift ( $z < 2$ ) QSO[XUV] and 268 higher redshifts ( $z > 2$ ) QSO[XUV] subsamples, respectively. Both constraints are consistent with each other,

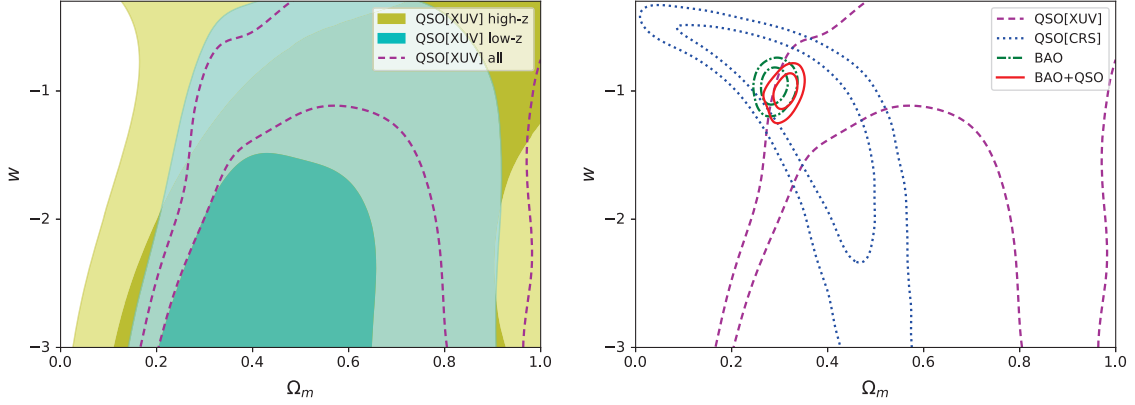


FIG. 5: Two-dimensional distributions of the  $w$ CDM model parameters ( $w$  and  $\Omega_m$ ). Left: The cyan and yellow contours indicate the constraints from 1330 low redshift QSO[XUV] and 268 high redshift QSO[XUV] data points, respectively. Right: The magenta dashed, blue dotted, green dash-dot, and red solid contours indicate the constraints from QSO[XUV], QSO[CRS], BAO, and BAO+QSO, respectively. Both figures assume the  $H_0 = 67.32 \pm 4.7 \text{ km s}^{-1} \text{ Mpc}^{-1}$  prior derived from Gaussian Process discussed in Section II.

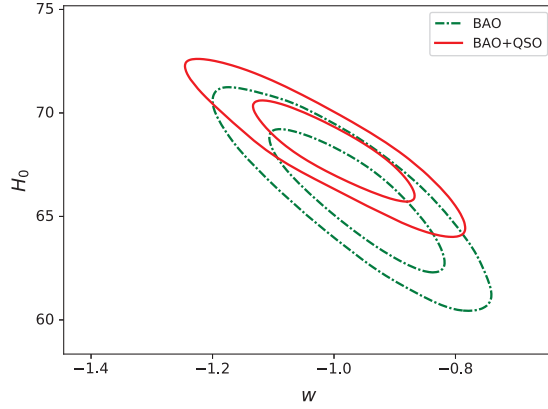


FIG. 6: Two-dimensional confidence contours of  $w$ CDM model parameters. The green dash-dot and red solid contours denote the constraints from BAO and BAO+QSO, respectively.

but the low redshift subsample provided a tighter result. This implies that extrapolating the calibrated nuisance parameters from lower to higher redshifts is effective. With the polynomial expansion  $P[\log(1+z)]$ , ref.[19] found the deviation between the concordance  $\Lambda$ CDM model and the whole QSO[XUV] data. Our results show that the  $\Lambda$ CDM model is at the edge of the  $2\sigma$  confidence region, which implies that the deviation still exists but is more moderate than in [19]. The validity of the polynomial expansions is still ambiguous, especially at high redshifts [47, 48], and this method requires great care. In the right panel of Fig.(5), the magenta dashed, blue dotted, green dash-dot, and red solid contours indicate the constraints from QSO[XUV], QSO[CRS], BAO, and BAO+QSO, respectively. The corresponding best-fitted values and their  $1\sigma$  uncertainties are summarized in Table.I. QSO[XUV] prefer large matter density and much smaller EoS parameter  $w$ , which is consistent with the result reported in ref.[36], where the constraining ability of 2015 [25] and 2019 [19] QSO[XUV] samples were compared. The QSO[CRS] sample showed similar limitations as SN Ia and preferred too large DE EoS parameters. It performed better than QSO[XUV] as a test for cosmological model parameters. The results show that adding both QSO[XUV] and QSO[CRS] (hereafter, abbreviated as QSO) can give much tighter constraint results (see the comparison of red and green contours in Fig.(5)). The degeneracy between the Hubble constant  $H_0$  and the DE EoS parameter  $w$  can also be observed in the BAO+QSO sample in Fig.(6). To some extent, it alleviates the discrepancy between the Hubble constant from the cosmological-model-dependent high-redshift observations and local-model-independent measurements.

It is hard to simultaneously determine the intercept parameter  $\beta$  for QSO[XUV] and the Hubble constant  $H_0$  according to Eq.(1). Moreover, the linear-size parameter  $l$  for QSO[CRS] and the Hubble constant  $H_0$  are degenerated

TABLE I: Best-fitted parameters for different dark energy models. We assumed the Gaussian prior distributions for the nuisance parameters:  $H_0 = \mathcal{N}(67.32, 4.7)$ ,  $\gamma = \mathcal{N}(0.634, 0.011)$ ,  $\beta = \mathcal{N}(7.75, 0.34)$  and  $\delta = \mathcal{N}(0.232, 0.005)$ .

| Model         | Data    | $\Omega_m$             | $w_0$                   | $w_a$                   | $\chi^2/d.o.f$ |
|---------------|---------|------------------------|-------------------------|-------------------------|----------------|
| $\Lambda$ CDM | BAO     | $0.28^{+0.03}_{-0.03}$ | -1                      | -                       | 7.28/10        |
| wCDM          | BAO     | $0.29^{+0.03}_{-0.03}$ | $-0.95^{+0.14}_{-0.15}$ | -                       | 7.32/9         |
| CPL           | BAO     | $0.30^{+0.06}_{-0.06}$ | $-0.88^{+0.42}_{-0.37}$ | $-0.27^{+1.29}_{-1.98}$ | 7.31/8         |
| JBP           | BAO     | $0.27^{+0.06}_{-0.07}$ | $-1.23^{+0.63}_{-0.69}$ | $1.99^{+3.44}_{-4.39}$  | 6.39/8         |
| Log           | BAO     | $0.31^{+0.05}_{-0.05}$ | $-0.84^{+0.35}_{-0.34}$ | $-0.29^{+0.79}_{-1.54}$ | 7.18/8         |
| Poly          | BAO     | $0.32^{+0.04}_{-0.05}$ | $0.38^{+0.86}_{-0.49}$  | $-0.21^{+0.28}_{-0.69}$ | 6.31/8         |
| $\Lambda$ CDM | BAO+QSO | $0.31^{+0.03}_{-0.03}$ | -1                      | -                       | 1967.05/1728   |
| wCDM          | BAO+QSO | $0.31^{+0.03}_{-0.03}$ | $-1.00^{+0.14}_{-0.13}$ | -                       | 1967.03/1727   |
| CPL           | BAO+QSO | $0.33^{+0.04}_{-0.04}$ | $-0.87^{+0.44}_{-0.31}$ | $-0.43^{+1.14}_{-1.88}$ | 1966.65/1726   |
| JBP           | BAO+QSO | $0.31^{+0.05}_{-0.04}$ | $-0.98^{+0.61}_{-0.50}$ | $0.02^{+2.87}_{-3.69}$  | 1967.14/1726   |
| Log           | BAO+QSO | $0.33^{+0.03}_{-0.03}$ | $-0.87^{+0.38}_{-0.28}$ | $-0.37^{+0.79}_{-1.36}$ | 1966.33/1726   |
| Poly          | BAO+QSO | $0.33^{+0.04}_{-0.04}$ | $0.41^{+0.74}_{-0.54}$  | $-0.24^{+0.32}_{-0.59}$ | 1964.99/1726   |

with each other according to Eq.(3). Hence, it is difficult to obtain the  $H_0$  value without a good prior knowledge of the nuisance parameters for QSO[XUV] or QSO[CRS]. Gravitational lensing provides a promising independent and a rather direct method of determining the Hubble constant  $H_0$ , and under the assumption of different cosmological models, it can be constrained from lensed quasars if the precision of the measurements is high enough. The time-delay distance of lensed quasars can be expressed as  $D_{\Delta t} = D_A(z_l)D_A(z_s)/D_A(z_l, z_s)$ , where  $z_l$  and  $z_s$  denote the redshifts of the lens and the source, respectively. Note that, in previous studies, another convention with the  $1 + z_l$  factor included in the  $D_{\Delta t}$  definition was widely used. The time-delay distance can be derived from time-delay measurements thus:  $\Delta t = (1 + z_l)D_{\Delta t}\Delta\phi$ , where  $\Delta\phi$ , called the Fermat potential difference, depends on the projected mass distribution of the lens and can be inferred from high-resolution imaging combined with spectroscopic observations and stellar kinematics of the lens galaxy. We employed the posterior probability distribution of  $D_{\Delta t}$  and  $D_A(z_l)$  from the H0LiCOW collaboration [17] and constrain the Hubble constant under the assumption of the DE EoS parametrizations discussed herein. The best fitted  $H_0$  are  $H_0^{\text{CPL}} = 81.3^{+5.1}_{-5.4}$   $\text{km s}^{-1} \text{Mpc}^{-1}$ ,  $H_0^{\text{JBP}} = 81.5^{+4.8}_{-5.5}$   $\text{km s}^{-1} \text{Mpc}^{-1}$ ,  $H_0^{\text{Log}} = 81.2^{+5.0}_{-5.0}$   $\text{km s}^{-1} \text{Mpc}^{-1}$  and  $H_0^{\text{Poly}} = 99.2^{+26.0}_{-15.3}$   $\text{km s}^{-1} \text{Mpc}^{-1}$  for the CPL, JBP, logarithmic, and Polynomial parametrizations, respectively. The lensed quasar sample can provide a promising constraint for  $H_0$ , but there is still a need to improve the precision before it could be employed in multiparameter cosmological model investigation, which is predicted to be achieved in the near future. However, in this study, the Hubble constant priors from the quasar sample were not employed, and we preferred to adopt  $H_0 = 67.32 \pm 4.7$   $\text{km s}^{-1} \text{Mpc}^{-1}$  from the reconstruction of the Hubble parameter measurements. The BAO itself also favored smaller Hubble constants, which is consistent with previous study [36, 59].

Our main focus was to investigate the DE EoS parameters; therefore, we used the Hubble parameters and BAO measurements to get tighter constraints for the Hubble constant  $H_0$  and the matter density  $\Omega_m$ . Obviously, the QSO sample can improve the constraining accuracy for all the parametrizations discussed in this work, as observed in Fig.(7). For comparison, we also included the  $\Lambda$ CDM model in this study. The detailed results are summarized in Table.(I). For more understanding, Fig.(8) shows the evolution of the DE EoS parameters according to different parameterizations following the joint BAO+QSO constraints. From the AIC and BIC criteria for the BAO+QSO constraints, the Polynomial parametrization is most favored, whereas the JBP parametrization is least favored among the two-parameter DE EoS parametrizations. The standard  $\Lambda$ CDM model exhibited the best performance. To quantify the constraining power of the quasar sample, we calculated the figure-of-merit (FoM) for the DE models with BAO only and BAO+QSO combined. The FoM can be expressed as

$$FoM = (\det Cov(\mathbf{p}))^{-1/2} \quad (23)$$

where  $Cov(\mathbf{p})$  is the covariance matrix of relevant cosmological parameters  $\mathbf{p}$ . The final FoM results are listed in Table(II), which also lists the relevant results of the information criteria and weights.

## V. CONCLUSION

Quasars are one of the brightest objects in the universe, and their cosmological redshift can be larger than  $z = 7$ . Therefore, they are natural candidates for standard cosmological probes. Several attempts have been made to use quasars as cosmological probes; however, their practical use as standard probes is still challenging. Currently, two

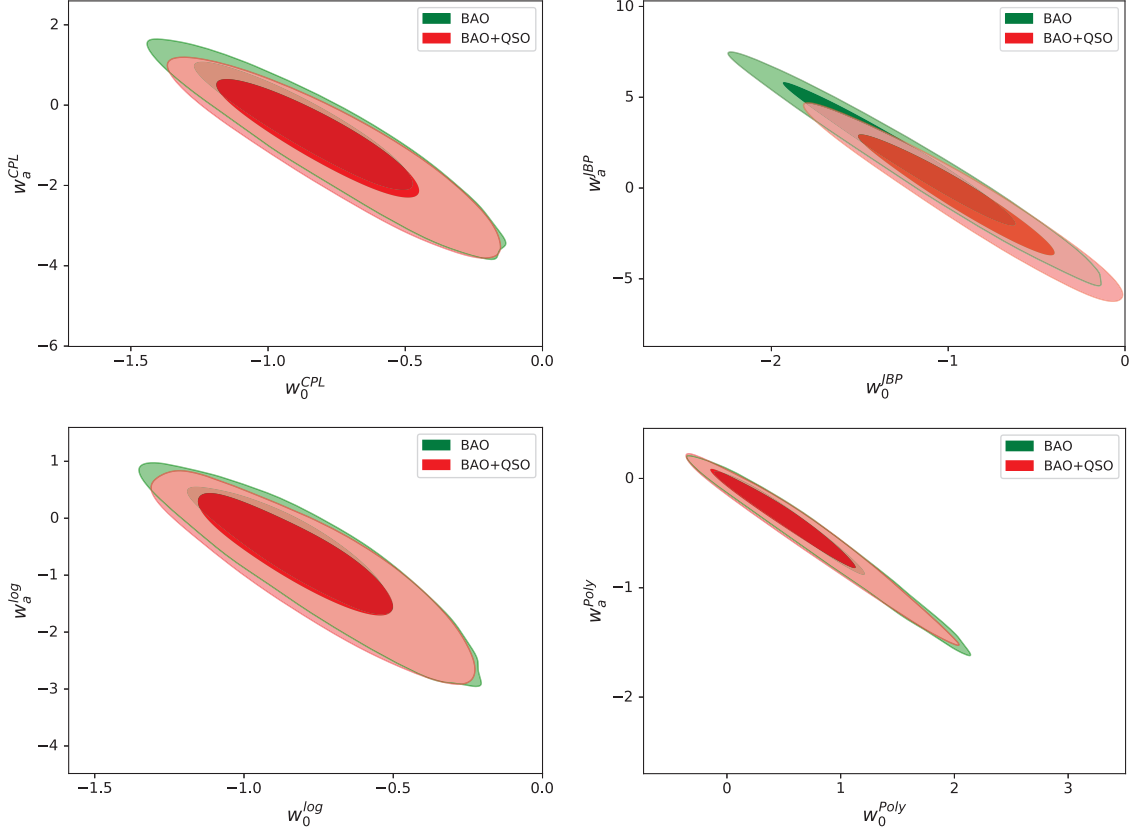


FIG. 7: Dark Energy Equation of State parameters constraint results with  $H_0 = 67.32 \pm 4.7 \text{ km s}^{-1} \text{ Mpc}^{-1}$  prior. The green and red contours denote BAO and BAO+QSO, respectively.

TABLE II: AIC and BIC information criteria (values, differences, weights) and the Figure-of-Merit for DE EoS parameters (pairwise and for all parameters).

| Model         | Data    | AIC <sub>i</sub> | $\Delta_i(\text{AIC})$ | $w_i(\text{AIC})$ | BIC <sub>i</sub> | $\Delta_i(\text{BIC})$ | $w_i(\text{BIC})$ | FoM( $w_0-w_a$ ) | FoM( $\mathbf{p}$ ) |
|---------------|---------|------------------|------------------------|-------------------|------------------|------------------------|-------------------|------------------|---------------------|
| $\Lambda$ CDM | BAO     | 9.28             | 0                      | 0.4838            | 9.68             | 0                      | 0.5646            | —                | 51.9                |
| wCDM          | BAO     | 11.32            | 2.04                   | 0.1744            | 12.12            | 2.44                   | 0.1667            | —                | 601.0               |
|               | CPL     | 13.31            | 4.03                   | 0.0645            | 14.50            | 4.82                   | 0.0507            | 8.4              | 439.1               |
|               | JBP     | 12.39            | 3.11                   | 0.1022            | 13.58            | 3.90                   | 0.0803            | 4.4              | 338.0               |
|               | Log     | 13.18            | 3.90                   | 0.0688            | 14.37            | 4.69                   | 0.0541            | 11.6             | 592.7               |
|               | Poly    | 12.31            | 3.03                   | 0.1063            | 13.50            | 3.82                   | 0.0836            | 29.5             | 2046.0              |
| $\Lambda$ CDM | BAO+QSO | 1969.05          | 0                      | 0.4466            | 1974.51          | 0                      | 0.9727            | —                | 95.1                |
| wCDM          | BAO+QSO | 1971.03          | 1.98                   | 0.1659            | 1981.94          | 7.43                   | 0.0237            | —                | 941.2               |
|               | CPL     | 1972.65          | 3.60                   | 0.0738            | 1989.02          | 14.51                  | 0.0007            | 8.9              | 827.0               |
|               | JBP     | 1973.14          | 4.09                   | 0.0578            | 1989.51          | 15.00                  | 0.0005            | 4.5              | 418.0               |
|               | Log     | 1972.33          | 3.28                   | 0.0866            | 1988.70          | 14.19                  | 0.0008            | 12.0             | 1101.1              |
|               | Poly    | 1970.99          | 1.94                   | 0.1693            | 1987.36          | 12.85                  | 0.0016            | 30.5             | 3049.9              |

classes of quasar samples appear to be promising. First, the nonlinear relation between the ultraviolet and X-ray luminosities of quasars (QSO[XUV] in short) can be used to derive luminosity distances. Second, the linear size of the compact radio structure in quasars (QSO[CRS] in short) can provide angular-diameter distances. These two processes have their respective advantages; however, they are challenged by their nuisance parameters, which demand clarification before they can be employed in any cosmological applications. In this study, we simultaneously refreshed the calibration of such parameters through a cosmological-model independent method in light of the newly compiled Hubble parameter sample for the two processes. The calibration results for the QSO[XUV] nuisance parameters are: the slope parameter  $\gamma = 0.634 \pm 0.011$ , the intercept  $\beta = 7.75 \pm 0.34$ , and the dispersion  $\delta = 0.232 \pm 0.005$ . These

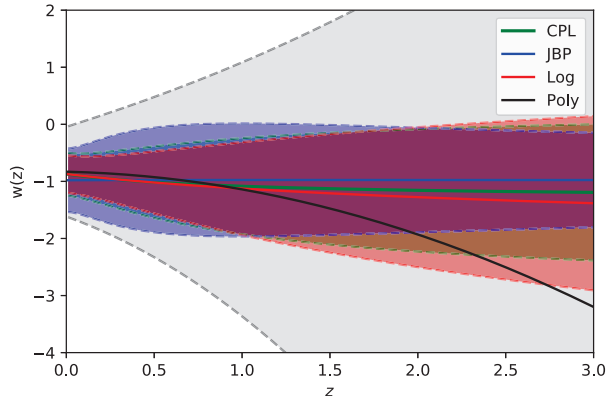


FIG. 8: Evolution of Dark Energy Equation of State parameters according to different parameterizations following the joint BAO+QSO constraint.

results are consistent with those of ref.[19] and fitted with the cosmological parameters with the nuisance parameters simultaneously [36]. For the QSO[CRS] linear-size Parameter,  $l = 10.89 \pm 0.19 pc$ , which is a little smaller than that calibrated with Hubble parameters in a redshift coverage of  $z < 1.2$  [27] and Union2.1 SN Ia in a redshift coverage of  $z < 1.4$  [28].

With the calibrated nuisance parameters, we tested and compared their abilities to constrain cosmological models. The results show that both quasar samples are promising complementary probes, and with the current measurement precision, the compact radio quasars perform better. The considerable degeneracy between  $w$  and  $H_0$  shows the importance of using complementary  $H_0$  measurements from quasar observations, such as gravitational lensing time-delay measurements, before DE EoS investigations. Both Hubble parameter measurements and BAO observations prefer smaller Hubble constants, and thus, we considered the  $H_0$  derived from the reconstruction of the Hubble parameter as a prior during the investigation. Moreover, with the calibrated quasar sample, we investigated four different DE EoS with  $H_0$  derived from the Gaussian Process reconstruction, the most recent baryon acoustic oscillation measurements, and both quasar samples. The results show that the quasar sample can improve the precision and the combined QSO+BAO measurements are consistent with the standard  $\Lambda$ CDM model. From the AIC and BIC values, among the four parametrizations discussed, the polynomial parametrization is most favored, whereas the JBP parametrization is least favored. In the future, samples of compact radio quasars and X-ray UV quasar data that are better controlled for systematics and with significantly lower dispersion would be helpful in the high-precision studies of dynamical DE models.

### Acknowledgments

This work was supported by the National Natural Science Foundation of China under Grant Nos. 12021003, 11690023, 11633001 and 11920101003, the National Key R&D Program of China (Grant No. 2017YFA0402600), the Beijing Talents Fund of Organization Department of Beijing Municipal Committee of the CPC, the Strategic Priority Research Program of the Chinese Academy of Sciences (Grant No. XDB23000000), the Interdiscipline Research Funds of Beijing Normal University, and the Opening Project of Key Laboratory of Computational Astrophysics, National Astronomical Observatories, Chinese Academy of Sciences. M.B. was supported by the Foreign Talent Introducing Project and Special Fund Support of Foreign Knowledge Introducing Project in China. He was supported by the Key Foreign Expert Program for the Central Universities No. X2018002. X. Li was supported by the National Natural Science Foundation of China (Grant Nos. 11947091, 12003006) and Hebei NSF (Grant No. A202005002).

---

[1] A. G. Riess, A. V. Filippenko, P. Challis, A. Clocchiattia, A. Diercks, P. M. Garnavich, R. L. Gilliland, C. J. Hogan, S. Jha, R. P. Kirshner, B. Leibundgut, M. M. Phillips, D. Reiss, B. P. Schmidt, R. A. Schommer, R. C. Smith, J. Spyromilio, C. Stubbs, N. B. Suntzeff, and J. Tonry, *Astron. J.* 116, 1009 (1998)

- [2] S. Perlmutter, et al. (The Supernova Cosmology Project), *Astrophys. J.* 517, 565 (1999)
- [3] N. Suzuki, et al. (The Supernova Cosmology Project), *Astrophys. J.* 746, 85 (2012)
- [4] M. Betoule, R. Kessler, J. Guy, J. Mosher, D. Hardin, R. Biswas, P. Astier, P. El-Hage, M. König, S. Kuhlmann, J. Marriner, R. Pain, N. Regnault, C. Balland, B. A. Bassett, P. J. Brown, H. Campbell, R. G. Carlberg, F. Cellier-Holzem, D. Cinabro, A. Conley, C. B. D'Andrea, D. L. DePoy, M. Doi, R. S. Ellis, S. Fabbro, A. V. Filippenko, R. J. Foley, J. A. Frieman, D. Fouchez, L. Galbany, A. Goobar, R. R. Gupta, G. J. Hill, R. Hlozek, C. J. Hogan, I. M. Hook, D. A. Howell, S. W. Jha, L. Le Guillou, G. Leloudas, C. Lidman, J. L. Marshall, A. Müller, A. M. Mourão, J. Neveu, R. Nichol, M. D. Olmstead, N. Palanque-Delabrouille, S. Perlmutter, J. L. Prieto, C. J. Pritchett, M. Richmond, A. G. Riess, V. Ruhlmann-Kleider, M. Sako, K. Schahmaneche, D. P. Schneider, M. Smith, J. Sollerman, M. Sullivan, N. A. Walton, and C. J. Wheeler, *Astron. Astrophys.* 568, A22 (2014)
- [5] D. M. Scolnic, D. O. Jones, A. Rest, Y. C. Pan, R. Chornock, R. J. Foley, M. E. Huber, R. Kessler, G. Narayan, A. G. Riess, S. Rodney, E. Berger, D.J. Brout, P. J. Challis, M. Drout, D. Finkbeiner, R. Lunnan, R. P. Kirshner, N. E. Sanders, E. Schlafly, S. Smartt, C. W. Stubbs, J. Tonry, W. M. Wood-Vasey, M. Foley, J. Hand, E. Johnson, W. S. Burgett, K. C. Chambers, P. W. Draper, K. W. Hodapp, N. Kaiser, R. P. Kudritzki, E. A. Magnier, N. Metcalfe, F. Bresolin, E. Gall, R. Kotak, M. McCrum, and K. W. Smith, *Astrophys. J.* 859, 101 (2018)
- [6] G. Hinshaw, et al. (WMAP Collaboration), *Astrophys. J.* S. 208, 19 (2013)
- [7] N. Aghamim, et al. (Planck Collaboration), arXiv: 1807.06209
- [8] P.A.R. Ade, et al. (Planck Collaboration), *Astron. Astrophys.* 594, A13 (2016)
- [9] D. J. Eisenstein, I. Zehavi, D. W. Hogg, R. Scoccamarro, M. R. Blanton, R. C. Nichol, R. Scranton, H. Seo, M. Tegmark, Z. Zheng, S. Anderson, J. Annis, N. Bahcall, J. Brinkmann, S. Burles, F. J. Castander, A. Connolly, I. Csabai, M. Doi, M. Fukugita, J. A. Frieman, K. Glazebrook, J. E. Gunn, J. S. Hendry, G. Hennessy, Z. Ivezić, S. Kent, G. R. Knapp, H. Lin, Y. Loh, R. H. Lupton, B. Margon, T. McKay, A. Meiksin, J. A. Munn, A. Pope, M. Richmond, D. Schlegel, D. Schneider, K. Shimasaku, C. Stoughton, M. Strauss, M. SubbaRao, A. S. Szalay, I. Szapudi, D. Tucker, B. Yanny, and D. York, *Astrophys. J.* 633, 560 (2005)
- [10] S. Alam, M. Ata, S. Bailey, F. Beutler, D. Bizyaev, J. A. Blazek, A. S. Bolton, J. R. Brownstein, A. Burden, C.-H. Chuang, J. Comparat, A. J. Cuesta, K. S. Dawson, D. J. Eisenstein, S. Escoffier, H. Gil-Marín, J. N. Grieb, N. Hand, S. Ho, K. Kinemuchi, D. Kirkby, F. Kitaura, E. Malanushenko, V. Malanushenko, C. Maraston, C. K. McBride, R. C. Nichol, M. D. Olmstead, D. Oravetz, N. Padmanabhan, N. Palanque-Delabrouille, K. Pan, M. Pellejero-Ibanez, W. J. Percival, P. Petitjean, F. Prada, A. M. Price-Whelan, B. A. Reid, S. A. Rodríguez-Torres, N. A. Roe, A. J. Ross, N. P. Ross, G. Rossi, J. A. Rubino-Martin, A. G. Sanchez, S. Saito, S. Salazar-Albornoz, L. Samushia, S. Satpathy, C. G. Scoccola, D. J. Schlegel, D. P. Schneider, H.-J. Seo, A. Simmons, A. Slosar, M. A. Strauss, M. E. C. Swanson, D. Thomas, J. L. Tinker, R. Tojeiro, M. V. Magana, J. A. Vazquez, L. Verde, D. A. Wake, Y.T. Wang, D. H. Weinberg, M. White, W. M. Wood-Vasey, C. Yèche, I.Zehavi, Z.-X. Zhai, and G.-B. Zhao, *Mon. Not. R. Astron. Soc.* 470, 2617 (2017)
- [11] M. Moresco, L. Pozzetti, A. Cimatti, R. Jimenez, C. Maraston, L. Verde, D. Thomas, A. Citro, R. Tojeiro, and D. Wilkinson, *J. Cosmol. Astropart. Phys.* 5, 014 (2016)
- [12] A.L. Ratsimbazafy, S.I. Loubser, S.M. Crawford, *Mon. Not. R. Astron. Soc.* 467, 3239 (2017)
- [13] S. Cao, Y. Pan, M. Biesiada, W. Godlowski, Z.H. Zhu, *J. Cosmol. Astropart. Phys.* 3, 16 (2012)
- [14] S. Cao, M. Biesiada, R. Gavazzi, A. Piórkowska, Z.H. Zhu, *Astrophys. J.* 806, 185 (2015)
- [15] A. G. Riess, L. M. Macri, S. L. Hoffmann, D. Scolnic, S. Casertano, A. V. Filippenko, B. E. Tucker, M. J. Reid, D. O. Jones, J. M. Silverman, R. Chornock, P. Challis, W. Yuan, P. J. Brown, and R. J. Foley, *Astrophys. J.* 826, 56 (2016)
- [16] A. G. Riess, S. Casertano, W. Yuan, L. M. Macri, and D. Scolnic, *Astrophys. J.* 876, 85 (2019)
- [17] K.C. Wong, et al. (H0LiCOW Collaboration), *Mon. Not. R. Astron. Soc.* 498, 1420 (2020)
- [18] X.G. Zheng, X.H. Ding, M. Biesiada, S. Cao, and Z.H. Zhu, *Astrophys. J.* 825, 17 (2016)
- [19] G. Risaliti, and E. Lusso, *Nat. Astron.*, 3, 274 (2019)
- [20] S. Cao, Z.H. Zhu, *Physical Review D*, 90, 083006 (2014)
- [21] D. Watson, K.D. Denney, M. Vestergaard, and T.M. Davis, *ApJL*, 740, L49 (2011)
- [22] M. L. Martínez-Aldama, B. Czerny, D. Kawka, V. Karas, S. Panda, M. Zająček, and P. T. Zycki, *Astrophys. J.* 883, 170 (2019)
- [23] J.M. Wang, P. Du, D. Valls-Gabaud, C. Hu, and H. Netzer, *Phys. Rev.Lett.* 110, 081301 (2013)
- [24] F. La Franca, S. Bianchi, G. Ponti, E. Branchini, and G. Matt, *Astrophys. J.* 787, L12 (2014)
- [25] G. Risaliti, and E. Lusso, *Astrophys. J.* 815, 33 (2015)
- [26] M. Elivs, and M. Karovska, *Astrophys. J.* 581, L67 (2002)
- [27] S. Cao, X.G. Zheng, M. Biesiada, J.Z. Qi, Y. Chen, and Z.H. Zhu, *Astron. Astrophys.* 606, A15 (2017a)
- [28] S. Cao, M. Biesiada, J. Jackson, X.G. Zheng, Y.H. Zhao, and Z.H. Zhu, *J. Cosmol. Astropart. Phys.* 02, 012 (2017b)
- [29] S. Cao, M. Biesiada, J. Qi, Y. Pan, X. Zheng, T. Xu, X. Ji, Z.H. Zhu, *Eur. Phys. J. C* 78, 749 (2018)
- [30] S. Cao, J.Z. Qi, M. Biesiada, T. Liu, Z.H. Zhu, *Astrophys. J. Lett.* 888, L25 (2020)
- [31] S. Cao, J.Z. Qi, M. Biesiada, X. Zheng, T. Xu, Y. Pan, Z.H. Zhu, *Physics of the Dark Universe*, 24, 100274 (2019)
- [32] X.G. Zheng, K. Liao, M. Biesiada, S. Cao, T.H. Liu, Z.H. Zhu, *Astrophys. J.* 892, 103 (2020)
- [33] M. Seikel, C. Clarkson, and M. Smith, *J. Cosmol. Astropart. Phys.* 06, 036 (2012)
- [34] F. Melia, *Mon. Not. R. Astron. Soc.* 489, 517 (2019)
- [35] N. Khadka, and B. Ratra, *Mon. Not. R. Astron. Soc.* 492, 4456 (2020)
- [36] N. Khadka, and B. Ratra, *Mon. Not. R. Astron. Soc.* 497, 263 (2020)
- [37] T.H. Liu, S. Cao, M. Biesiada, Y.T. Liu, S.B. Geng, and Y.J. Lian, *Astrophys. J.* 899, 71 (2020)
- [38] J.J. Wei, and F. Melia, *Astrophys. J.* 897, 127 (2020)

- [39] K.I. Kellermann, *Nature*, 361, 134 (1993)
- [40] L.I. Gurvits, *Astrophys. J.* 425, 442 (1994)
- [41] L.I. Gurivts, *Astron. Astrophys.* 342, 378 (1999)
- [42] J.Z. Qi, S. Cao, M. Biesiada, X. Zheng, Z.H. Zhu, *Eur. Phys. J. C*, 77, 502 (2017)
- [43] X. Zheng, M. Biesiada, S. Cao, J. Qi, Z.H. Zhu, *J. Cosmol. Astropart. Phys.* 10, 030 (2017)
- [44] T. Xu, S. Cao, J.Z. Qi, M. Biesiada, X. Zheng, Z.H. Zhu, *J. Cosmol. Astropart. Phys.* 06, 042 (2018)
- [45] Z.Y. Yin, and H. Wei, *Sci. China-Phys. Mech. Astron.* 62, 999811 (2019)
- [46] L. Amati, R. D'Agostino, O. Luongo, M. Muccino, and M. Tantalò, *Mon. Not. R. Astron. Soc.*, 486, L46 (2019)
- [47] A. Banerjee, E. Ó Colgáin, M. Sasaki, M. M. Sheikh-Jabbari, and T. Yang, arXiv:2009.04109
- [48] T. Yang, A. Banerjee, and E. Ó Colgáin, arXiv:1911.01681
- [49] H. Yu, B. Ratra, and F.Y. Wang, *Astrophys. J.* 856, 3 (2018)
- [50] A. Gómez-Valent, and L. Amendola, *J. Cosmol. Astropart. Phys.* 04, 051 (2018)
- [51] K. Liao, Z.X. Li, J. Ming, and Z.H. Zhu, 2013, *Phys. Lett. B.* 718, 1166 (2013)
- [52] M. Chevallier, and D. Polarski, *Int. J. Mod. Phys. D* 10, 213 (2001)
- [53] E.V. Linder, *Phys.Rev.Lett.*, 90, 091301 (2003)
- [54] H.K. Jassal, J.S. Bagla, and T. Padmanabhan, *Mon. Not. R. Astron. Soc.* 356, L11 (2005)
- [55] G. Efstathiou, *Mon. Not. R. Astron. Soc.* 310, 842 (1999)
- [56] J. Weller, and A. Albrecht, *Phys.Rev.D*, 65, 103512 (2002)
- [57] J. Ryan, S. Doshi, and B. Ratra, *Mon. Not. R. Astron. Soc.* 488, 3844 (2019)
- [58] A.R. Liddle, *Mon. Not. R. Astron. Soc.* 377, L74 (2007)
- [59] X. Zhang, and Q.G. Huang, *Sci. China Phys. Mech. Astron.* 63, 290402 (2020)